ChemComm

COMMUNICATION

View Article Online
View Journal | View Issue

Cite this: *Chem. Commun.*, 2016, **52**, 9450

Received 25th May 2016,
Accepted 28th June 2016

DOI: 10.1039/c6cc04387a

www.rsc.org/chemcomm

The surface sulfur doping induced enhanced performance of cobalt catalysts in oxygen evolution reactions†

Mohammad Al-Mamun,[a] Zhengju Zhu,[a] Huajie Yin,[a] Xintai Su,[ab] Haimin Zhang,[c] Porun Liu,[a] Huagui Yang,[a] Dan Wang,[a] Zhiyong Tang,[a] Yun Wang*[a] and Huijun Zhao*[ac]

A novel surface sulfur (S) doped cobalt (Co) catalyst for the oxygen evolution reaction (OER) is theoretically designed through the optimisation of the electronic structure of highly reactive surface atoms which is also validated by electrocatalytic OER experiments.

Recently, the electrocatalytic oxygen evolution reaction (OER) has attracted great attention since it is an important pathway to generate molecular oxygen for many energy conversion and storage applications, such as hydrogen generation *via* water hydrolysis and rechargeable metal–air batteries.[1] Since cobalt (Co)-based materials have been widely explored in many electrocatalytic processes due to their intrinsic electronic properties and earth-abundance[2] the Co-based catalysts have been investigated as a promising candidate for OERs.[3] The good performance of Co nanoparticles (NPs) in OERs has been reported by Wu *et al.*[4] However, the multistep preparation method is relatively complex and requires reductive annealing during the synthesis of Co NPs. In addition, Co catalysts have been oxidised before the water oxidation takes place. Thus, the real active composition for the catalytic OER process is unclear. Furthermore, the stability of this catalyst is relatively low and the performance drops 13% after 1 hour of electrocatalysis.[4] Up to this point, the synthesis of stable Co catalysts through a facile approach becomes attractive for OERs.

First, we need to understand the performance of Co catalysts in OERs. Generally, the performance of catalysts is determined by several key parameters, such as the reactivity of catalysts. To understand the reactivity of metallic Co catalysts for OERs, first-principles density functional theory (DFT) calculations are conducted to investigate the Gibbs free energy (ΔG) of four primitive steps of the OER process: adsorption (ΔG_1), dissociation (ΔG_2 and ΔG_3) and desorption (ΔG_4) by the method proposed by Nørskov *et al.*,[5] which are shown in Fig. 1a. The adsorption of three important intermediates: *O, *OH and *OOH on the Co(111) surface are investigated with the consideration of spin-polarisation and ferromagnetic structures (see Fig. 1b). It is found that the energy barrier (ΔG_3) for the formation of *OOH (3.45 eV) is about 3 times higher than the optimal value (1.23 eV from experiments, and 1.25 eV from theoretical results). This large ΔG_3 value is ascribed to the strong binding between *O and the catalyst surface. And the strong adsorption of *O is originated from the high reactivity of

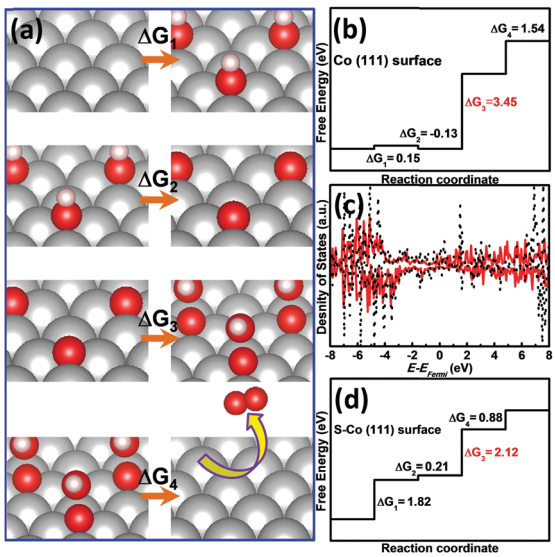

Fig. 1 (a) Primitive steps of the OER process on the Co(111) surface. Colour scheme for chemical representation: grey for Co, red for O and light pink for H; (b) standard Gibbs free energy diagram of the OER process on the Co(111) surface; (c) PDOS of Co 4s states on the Co(111) surface before (black dotted line) and after (red line) S-doping; and (d) standard Gibbs free energy diagram of the OER process on the S-doped Co(111) surface.

[a] *Centre for Clean Environment and Energy, Griffith University, Gold Coast Campus, QLD 4222, Australia. E-mail: yun.wang@griffith.edu.au, h.zhao@griffith.edu.au; Fax: +61 7 5552 8067; Tel: +61 7 5552 8261*

[b] *Ministry Key Laboratory of Oil and Gas Fine Chemicals, College of Chemistry and Chemical Engineering, Xinjiang University, Urumqi 830046, P. R. China*

[c] *Centre for Environmental and Energy Nanomaterials, Institute of Solid State Physics, Chinese Academy of Sciences, Hefei 230031, P. R. China*

† Electronic supplementary information (ESI) available: Experimental section and characterisation. See DOI: 10.1039/c6cc04387a

surface Co atoms. Thus, reducing the reactivity of the surface atoms is required to optimise the OER performance of Co metal based catalysts.

Previous studies have demonstrated that the reactivity is in principle governed by the electronic structures of the catalysts.[6] To this end, novel catalysts can be molecularly designed by engineering their electronic structures. One doable way to manipulate the electronic structures of metal surface atoms is through the introduction of modifiers onto the top surface.[7] In the petrochemical industry, sulfur (S) has been criticised to irreversibly poison the transition metal catalysts by reducing the reactivity of surface atoms.[8] In this regard, S can be introduced here to reduce the reactivity of metallic Co catalysts. Herein, our DFT calculations demonstrate that the electronic structures of metallic Co catalysts can be changed through surface S-doping to improve their catalytic performance in OERs, which is further validated by our electrocatalytic OER experiments.

The effects of adsorbed S atoms on the electronic properties of the Co(111) surface are first studied through the analysis of the partial density of states (PDOS) of surface Co 4s states based on the DFT results at the generalised gradient approximation (GGA) level (see Fig. 1c). Co 4s states are focused since 4s is the outermost valence orbital of Co atoms, which largely determines their reactivity. The major spin components of all Co atoms are kept in the same direction since it is the most stable magnetic structure based on our calculations; and the coverage of S (θ, which is defined as the ratio between the adsorbed S and the surface Co atoms) is 0.5. It can be found that the peaks of Co 4s states around the Fermi energy level becomes lower and wider after the adsorption of S atoms. Since the sharp peaks around the Fermi energy mean the atoms are more reactive,[9] the change of PDOS of surface Co 4s states suggests that the reactivity of Co surface atoms can be reduced by S-doping, which may benefit the optimisation of adsorption–desorption energies of the intermediates of OERs. In addition, the adsorption energies of *O are −2.53 and −0.54 eV on the Co(111) surface without and with S-doping, respectively, whereas the negative values imply the exothermic nature of the adsorption process. The significantly increased adsorption energy further supports the dramatic reduction of the reactivity of surface Co atoms *via* S-doping.

Employing the same method proposed by Nørskov *et al.*,[5] the Gibbs free energies of four primary steps of electrocatalytic OERs on the S-doped surface are calculated. The Gibbs free energy diagrams at various stages of the OER process are shown in Fig. 1b and d. After S-doping, the ΔG_1 value increases by about 12 times. The increased ΔG_1 value is also ascribed to the weak adsorption of *OH, which is caused by the reduced reactivity of surface Co atoms by S-doping. Moreover, the weak adsorption of *O leads to the formation of *OOH on the surface becomes much easier. As a result, the ΔG_3 value decreases by 39% after S-doping. The theoretical overpotential can be calculated by the division between the maximum difference of ΔG_n (n = 1–4) and the optimal value (1.25 eV from the theoretical calculations) and electron charge. It can be found that the theoretical overpotential can be changed from 2.20 V to 0.86 V after S-doping based on the Gibbs free energy diagram (Fig. 1b and d).

Inspired by the theoretical prediction, the surface S-doped Co nanoparticles (S-Co NPs) supported on the carbon nanosheet (S-Co/CNS) is synthesised through a one-step molten-salt calcination of the $Co(OH)_2$/OA precursor (see the Experimental section for details, ESI†) at 500 °C in a tubular furnace under Ar protection. For a meaningful comparison, pure Co NPs on CNS (denoted as Co/CNS) was also prepared.

The X-ray diffraction (XRD) patterns of Co/CNS and S-Co/CNS in Fig. 2a display three peaks at 44.2, 51.5 and 75.8°, corresponding to (111), (200) and (220) planes of the face-centered cubic (fcc) metallic Co crystal structure (JCPDS 15-0806). Apparently, similar XRD patterns suggest that the bulk crystalline structures of the both catalysts are metallic Co. Raman spectroscopic measurements of Co/CNS and S-Co/CNS samples further confirm the formation of metallic Co NPs on the CNS with the characteristic peaks at 189.6, 467.5, 504.4 and 668.6 cm^{-1} for Co NPs along with the D and G bands at 1346.3 and 1589.8 cm^{-1} for distorted graphitic carbon (Fig. 2b).[10]

The SEM images (Fig. 2c) of S-Co/CNS show the surface microstructures of the prepared sample composed of S-Co NPs with a CNS thickness of ~50 nm (Fig. 2c, inset). As shown, the S-Co NPs having sizes from 30 to 40 nm are uniformly distributed on the CNS (Fig. 2c) and these S-Co NPs connected closely with CNS might improve the overall conductivity of the catalyst when used as an electrocatalyst for OER. The S-Co NPs can be clearly distinguished in Fig. 2d, which indicates a negligible aggregation of NPs at this elevated temperature (500 °C). The high-resolution TEM (HRTEM) technique is also employed to observe the lattice spacing of 0.21 nm, which demonstrates that the mostly exposed facet of Co NPs is the (111) plane (Fig. 2d, bottom left).

Fig. 3a and b display the bright- and dark-field TEM images of the as synthesised S-Co/CNS sample where S-Co NPs can be

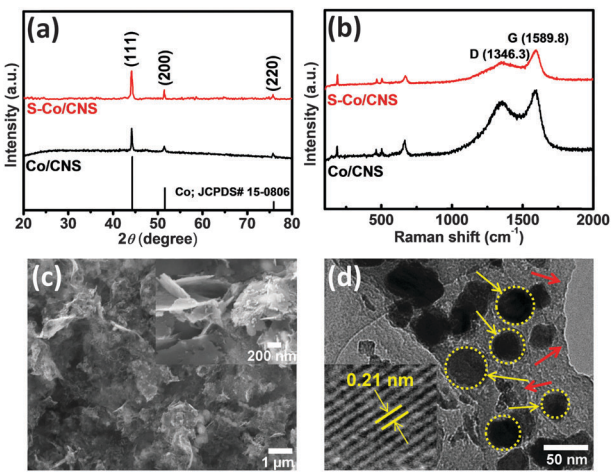

Fig. 2 (a) XRD pattern and (b) Raman spectra of Co/CNS and S-Co/CNS samples; (c) SEM and (d) TEM images of the S-Co/CNS sample. Insets of (c) and (d) (bottom left) show the high magnification SEM and local HRTEM images, respectively. Yellow and red arrows in (d) indicate the S-Co NPs and CNS, respectively.

identified on CNS. Meanwhile, the energy dispersive X-ray spectroscopy (EDS) mapping is conducted to visualise the elemental distribution throughout the catalyst. As shown in Fig. 3c, the NPs are composed of Co and S where the CNS acts as a supporting conducting substrate. Interestingly, the elemental S can only be detected on the Co species and no S is observed on the carbon. It indicates that the S can only interact with Co metal as evidenced by the XPS study (Fig. 3d and e). On the basis of the aforementioned characterisations, we can demonstrate that S has been successfully doped on the Co NP surface in the S-Co/CNS sample without changing the bulk crystalline structure of Co NPs. For comparison purpose, EDS mapping is also conducted for the Co/CNS sample and no S is detected on the Co NP surface (Fig. S3, ESI†).

To investigate the surface S-doping mechanism, a mass spectrometer (MS) is employed to monitor the real time emitted gases (H_2O, CO, H_2S and CO_2) during the calcination of the $Co(OH)_2$/OA precursor. (Fig. S4, ESI†). The initial thermal decomposition (200–300 °C) of the $Co(OH)_2$/OA precursor produces cobalt oxide (Fig. S5, ESI†), carbon and water vapour as by-products. Thereafter, the simultaneous carbothermal reduction (300–500 °C) of both Na_2SO_4 and cobalt oxide might result in the formation of Na_2S and the Co metal. In addition, the hydrolysis of Na_2S can generate H_2S gas, which selectively sulfurises the metallic Co NPs surface to form S-Co/CNS catalyst (see the chemical reactions, ESI†).

To understand the surface properties of S-Co/CNS catalysts, X-ray photoelectron spectroscopy (XPS) measurements are conducted. The comparative surface survey spectra of Co/CNS and S-Co/CNS (Fig. 3d) demonstrate the presence of common elements such as Co, C and O in both samples, whereas S can only be detected in the S-Co/CNS sample. The surface elemental contents of the S-Co/CNS sample are Co 4.06%, S 1.98%, C 47.99% and O 45.98%, which means the surface coverage of S is ~0.50 on the Co(111) surface. Thus, we can use the experimental data to validate the theoretical results since they are obtained under similar conditions. As shown in Fig. 3e, the Co $2p_{3/2}$ and $2p_{1/2}$ doublet peaked at 778.8 and 793.8 eV with the split spin–orbit of ~15 eV confirms the dominant Co^0 states in the Co/CNS sample.[11] On the other hand, the Co 2p doublet peaks are found to be slightly shifted to a higher binding energy and located at 779.9 and 795.6 eV with a split spin–orbit of ~15.7 eV for the S-Co/CNS sample, indicating the presence of oxidised states of Co atoms after S-doping, which is consistent with the literature.[12] Therefore, the oxidised Co species in the S-Co/CNS sample are presumed to be covalently bonded with the host S atoms derived from the H_2S gas evolved during the calcination. The Co–S bond formation is further demonstrated from the observed S $2p_{3/2}$ peak located at 162.4 eV (S^{2-} species) and 163.6 eV (S_n^{2-} species) in the S-Co/CNS sample (Fig. 3f).[7d] In this regard, the adsorption of S can significantly change the electronic properties of surface Co atoms, which is in agreement with the conclusions drawn from the theoretical PDOS analysis (see Fig. 1c).

The electrocatalytic OER performance of S-Co/CNS and other control samples including Co/CNS and benchmark RuO_2 catalysts are evaluated in alkaline solution (1.0 M KOH) using a standard three electrode system (see the Characterisation Section, ESI†). As displayed in Fig. 4a, the S-Co/CNS electrode displays the earliest onset potential of ≈1.46 V (*vs.* RHE) out of all catalysts studied in this work. Remarkably, the overpotential required to reach the current density of 10 mA cm^{-2} is 320 mV for the S-Co/CNS electrode, which is 134 mV and 15 mV lower than those of Co/CNS and RuO_2, respectively. The earliest onset

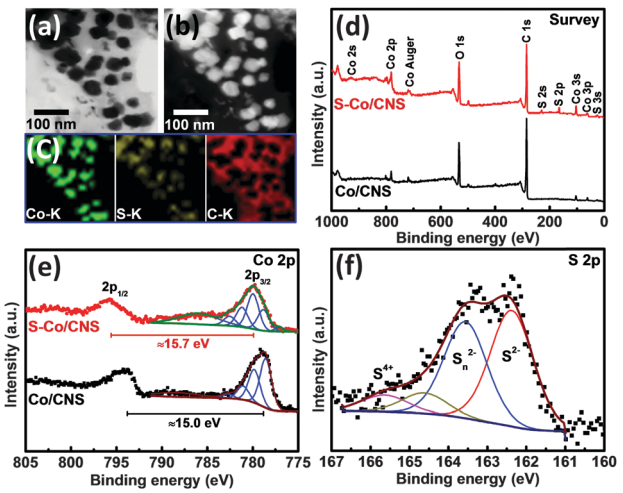

Fig. 3 (a) Bright-field, (b) dark-field TEM and (c) Co, S and C elemental distribution mapping of the S-Co/CNS sample; (d) survey, (e) high resolution Co 2p XPS spectra of Co/CNS and S-Co/CNS samples; and (f) S 2p spectrum of the S-Co/CNS sample.

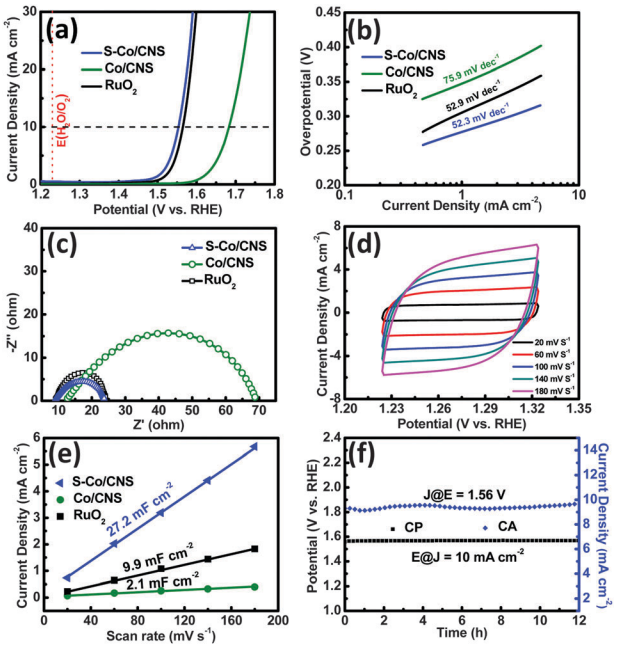

Fig. 4 (a) Polarisation curves, (b) Tafel plots and (c) Nyquist plots of Co/CNS, S-Co/CNS and RuO_2 electrocatalysts; (d) cyclic voltammograms of the S-Co/CNs electrocatalyst at scan rates from 20 to 180 mV s^{-1}; (e) plots of current densities at 1.275 V *vs.* scan rates of Co/CNS, S-Co/CNS and RuO_2 electrocatalysts; (f) chronopotentiometric (CP) and chronoamperometric (CA) plots of the S-Co/CNS electrocatalyst.

potential and lowest overpotential suggest that the intrinsic catalytic ability of S-Co/CNS has been greatly improved after S-doping, which therefore validates the theoretical prediction.

To evaluate the OER kinetics, Tafel plots are constructed and shown in Fig. 4b. It can be seen that the S-Co/CNS exhibits superior OER kinetics as evidenced by its small Tafel slope of 52.3 mV dec^{-1}, which is much lower than that of Co/CNS (75.9 mV dec^{-1}) and even slightly smaller than that of RuO_2 (52.9 mV dec^{-1}). To explain such superior kinetics of S-Co/CNS, the electrochemical impedance spectroscopy (EIS) is employed to examine the charge transfer process of the catalysts. As shown in Fig. 4c, the charge transfer resistance (R_{ct}) of S-Co/CNS (14.1 Ω) is much smaller than that of Co/CNS (56.6 Ω) and merely similar to that of RuO_2 (14.2 Ω), consistent with the Tafel measurements. The electrochemical double-layer capacitance (C_{dl}) values of the electrocatalysts are also measured under the non-Faradic potential window and are presented in Fig. 4e. The resulting C_{dl} value of S-Co/CNS is 27.2 mF cm^{-2}, whereas the C_{dl} values of Co/CNS and RuO_2 are calculated to be only 2.1 and 9.9 mF cm^{-2}, respectively. The highest C_{dl} value of the S-Co/CNS electrocatalyst indicates the larger amount of charged species at the liquid/solid interface as confirmed by XPS analysis.[13,14] These accumulated charges on the catalyst surface might be also beneficial for the optimisation of the desorption energy for the electrocatalytic product (O_2) and thereby superior OER catalytic performance. As a result, the overpotential from the experiments is better than that of the theoretical values since they are obtained based on the oversimplified atomistic models.

Besides the thermodynamic and kinetic properties, the electrocatalytic stability is also important for their overall performance. As displayed in Fig. 4f, the chronopotentiometric (CP) and chronoamperometric (CA) plots of S-Co/CNS show impressive durability in the 1.0 M KOH electrolyte. The potential remains ≈1.56 V at 10 mA cm^{-2} for 12 h in the CP test, while the current density keeps close to ≈10 mA cm^{-2} at 1.56 V for the entire testing duration in the CA test.

In summary, our DFT results predict that the surface S-doping can significantly improve the OER performance of Co catalysts. Accordingly, our experiments confirm that the S-Co/CNS catalyst possesses excellent electrocatalytic properties for OER. Our results may illustrate a new paradigm for the development of advanced electrocatalysts for energy conversion and storage applications.

This work was financially supported by Australian Research Council (ARC) Discovery Project and the National Natural Science Foundation of China (Grant No. 51372248 and 51432009). All the DFT calculations were conducted in the National Computational Infrastructure (NCI) of Australia.

Notes and references

1 (*a*) B. Zhang, X. Zheng, O. Voznyy, R. Comin, M. Bajdich, M. García-Melchor, L. Han, J. Xu, M. Liu, L. Zheng, F. P. García de Arquer, C. T. Dinh, F. Fan, M. Yuan, E. Yassitepe, N. Chen, T. Regier, P. Liu, Y. Li, P. De Luna, A. Janmohamed, H. L. Xin, H. Yang, A. Vojvodic and E. H. Sargent, *Science*, 2016, DOI: 10.1126/science.aaf1525; (*b*) S. Dresp, F. Luo, R. Schmack, S. Kuhl, M. Gliech and P. Strasser, *Energy Environ. Sci.*, 2016, **9**, 2020; (*c*) M. G. Walter, E. L. Warren, J. R. McKone, S. W. Boettcher, Q. Mi, E. A. Santori and N. S. Lewis, *Chem. Rev.*, 2010, **110**, 6446; (*d*) J. Luo, J. H. Im, M. T. Mayer, M. Schreier, M. K. Nazeeruddin, N. G. Park, S. D. Tilley, H. J. Fan and M. Grätzel, *Science*, 2014, **345**, 1593; (*e*) X. Zhang, R. Liu, Y. Zang, G. Liu, G. Wang, Y. Zhang, H. Zhang and H. Zhao, *Chem. Commun.*, 2016, **52**, 5946; (*f*) T. Y. Ma, J. L. Cao, M. Jaroniec and S. Z. Qiao, *Angew. Chem., Int. Ed.*, 2016, **55**, 1138; (*g*) T. Y. Ma, J. Ran, S. Dai, M. Jaroniec and S. Z. Qiao, *Angew. Chem., Int. Ed.*, 2015, **54**, 4646; (*h*) S. Chen, J. Duan, P. Bian, Y. Tang, R. Zheng and S. Z. Qiao, *Adv. Energy Mater.*, 2015, **5**, 1500936; (*i*) S. Chen, J. Duan, Y. Tang, B. Jin and S. Zhang Qiao, *Nano Energy*, 2015, **11**, 11; (*j*) J. Duan, S. Chen, M. Jaroniec and S. Z. Qiao, *ACS Catal.*, 2015, **5**, 5207.

2 (*a*) G. Wu, K. L. More, C. M. Johnston and P. Zelenay, *Science*, 2011, **332**, 443; (*b*) S. Gao, Y. Lin, X. Jiao, Y. Sun, Q. Luo, W. Zhang, D. Li, J. Yang and Y. Xie, *Nature*, 2016, **529**, 68.

3 (*a*) X. Li, Z. Niu, J. Jiang and L. Ai, *J. Mater. Chem. A*, 2016, **4**, 3204; (*b*) X. Zou, J. Su, R. Silva, A. Goswami, B. R. Sathe and T. Asefa, *Chem. Commun.*, 2013, **49**, 7522; (*c*) X. Long, S. Xiao, Z. Wang, X. Zheng and S. Yang, *Chem. Commun.*, 2015, **51**, 1120; (*d*) M. Al-Mamun, X. Su, H. Zhang, H. Yin, P. Liu, H. Yang, D. Wang, Z. Tang, Y. Wang and H. Zhao, *Small*, 2016, **12**, 2866.

4 L. Wu, Q. Li, C. H. Wu, H. Zhu, A. Mendoza-Garcia, B. Shen, J. Guo and S. Sun, *J. Am. Chem. Soc.*, 2015, **137**, 7071.

5 (*a*) J. Rossmeisl, Z. W. Qu, H. Zhu, G. J. Kroes and J. K. Nørskov, *J. Electroanal. Chem.*, 2007, **607**, 83; (*b*) J. Rossmeisl, A. Logadottir and J. K. Nørskov, *Chem. Phys.*, 2005, **319**, 178.

6 (*a*) J. K. Nørskov, T. Bligaard, J. Rossmeisl and C. H. Christensen, *Nat. Chem.*, 2009, **1**, 37; (*b*) Y. Li, H. Zhang, Y. Wang, P. Liu, H. Yang, X. Yao, D. Wang, Z. Tang and H. Zhao, *Energy Environ. Sci.*, 2014, **7**, 3720.

7 (*a*) C. H. Cui and S. H. Yu, *Acc. Chem. Res.*, 2013, **46**, 1427; (*b*) Y. Wang, W. Wang, K. Fan and J. Deng, *Surf. Sci.*, 2001, **487**, 77; (*c*) Y. Wang, H. Zhang, P. Liu, T. Sun, Y. Li, H. Yang, X. Yao and H. Zhao, *J. Mater. Chem. A*, 2013, **1**, 12948; (*d*) Z. Tan, P. Liu, H. Zhang, Y. Wang, M. Al-Mamun, H. G. Yang, D. Wang, Z. Tang and H. Zhao, *Chem. Commun.*, 2015, **51**, 5695.

8 (*a*) J. Dunleavy, *Platinum Met. Rev.*, 2006, **50**, 110; (*b*) M. D. Argyle and C. H. Bartholomew, *Catalysts*, 2015, **5**, 145; (*c*) C. Bartholomew, P. Agrawal and J. Katzer, *Adv. Catal.*, 1982, **31**, 135.

9 G. J. Miller, *Angew. Chem., Int. Ed.*, 1989, **101**, 1570.

10 W. Zhou, J. Zhou, Y. Zhou, J. Lu, K. Zhou, L. Yang, Z. Tang, L. Li and S. Chen, *Chem. Mater.*, 2015, **27**, 2026.

11 M. C. Biesinger, B. P. Payne, A. P. Grosvenor, L. W. M. Lau, A. R. Gerson and R. S. C. Smart, *Appl. Surf. Sci.*, 2011, **257**, 2717.

12 M. A. White, T. C. Lovejoy, S. T. Ochsenbein, M. A. Olmstead and D. R. Gamelin, *J. Appl. Phys.*, 2010, **107**, 103917.

13 T. Audichon, T. W. Napporn, C. Canaff, C. Morais, C. Comminges and K. B. Kokoh, *J. Phys. Chem. C*, 2016, **120**, 2562.

14 S. Ardizzone and S. Trasatti, *Adv. Colloid Interface Sci.*, 1996, **64**, 173.